Journal of Solid State Chemistry **161,** 274–287 (2001)
doi:10.1006/jssc.2001.9308, available online at http://www.idealibrary.com IDEAL®

Characterization of New 5M and 7M Polytypes of Niobia-Doped $Ca_2Ta_2O_7$

I. E. Grey,*,[1] R. S. Roth,† W. G. Mumme,* J. Planes,‡ L. Bendersky,† C. Li,* and J. Chenavas§

** CSIRO Minerals, Box 312 Clayton South, Victoria 3169, Australia; † National Institute of Standards and Technology, Gaithersburg, Maryland 20899; ‡ Commissariat a l'Energie Atomique DSM/DRFMC, 38054 Grenoble, France; and § CNRS Laboratoire de Cristallographie, BP166, 38042 Grenoble, France*

Received January 23, 2001; in revised form July 6, 2001; accepted July 12, 2001

Two new calcium tantalate polytypes have been prepared in the system $Ca_2Ta_2O_7$–$Ca_2Nb_2O_7$. Their structures have been determined and refined using single-crystal X-ray diffraction data and powder neutron diffraction data, and their dielectric properties have been measured in the 100 kHz to 10 GHz frequency range. The 7M polytype of pure $Ca_2Ta_2O_7$ has monoclinic symmetry with $a = 12.726(1)$, $b = 7.380(1)$, $c = 42.538(1)$ Å, $\beta = 95.77(1)^\circ$, $Z = 28$, space group $C2$. The 7M $Ca_2Ta_{1.9}Nb_{0.1}O_7$ is isostructural, with $a = 12.7170(6)$, $b = 7.3728(3)$, $c = 42.464(2)$ Å, $\beta = 95.755(5)^\circ$. The 5M $Ca_2Ta_{1.8}Nb_{0.2}O_7$ is monoclinic with $a = 12.7528(4)$, $b = 7.3492(2)$, $c = 30.2442(8)$ Å, $\beta = 94.245(2)^\circ$, $Z = 20$, space group $C2$. The two polytypes have in common a closest-packing of (001) metal atom layers that alternately have the composition Ca_3Ta and Ca_3Ta. The polytypes have mixed hexagonal-cubic stacking sequences of the metal atom layers: 7M = *hccccchccccccch* ... , 5M = *hccchccccch* ... . The cubic-stacked blocks have weberite-type structures in both polytypes, in which hexagonal tungsten bronze type layers of corner-connected octahedra are interconnected via corner linking to isolated TaO_6 octahedra in the Ca_3Ta layers to give a $[Ta_2O_7]^{4-}$ framework within which the eight-coordinated calcium atoms are distributed. The polytypes display a broad resonance at about 8 GHz, with relative permittivities of ~ 25 and with Q values of about 200.

INTRODUCTION

The doping of calcium tantalate, $Ca_2Ta_2O_7$, with niobia in the system $Ca_2Ta_2O_7$–$Ca_2Nb_2O_7$ has been reported to produce materials with potentially useful dielectric properties (1). In particular, substitution of Nb for Ta results in an increase in the dielectric constant from 25 to ~ 35 at 1 MHz and the doping can be adjusted to give temperature coefficients of the dielectric constant close to zero, making the system worthy of further investigation for possible microwave communications applications. The interpretation of the observed changes in dielectric properties was limited because no phase or structure information was available at the time for either the niobia-doped samples or the end-member calcium tantalate.

We have recently reported the results of characterization studies on pure and substituted $Ca_2Ta_2O_7$ (2, 3). We noted that $Ca_2Ta_2O_7$ has a trigonal weberite-type (4) structure below 1400°C, with $a_{trig} = 7.355(1)$ Å and $c_{trig} = 18.09(1)$ Å. This is a fluorite-derivative structure comprising cubic stacking along [001] of close-packed metal atom layers ($\equiv \{111\}_{fluorite}$) where the layers alternately have the compositions Ca_3Ta and Ta_3Ca. Ordered occupation of 7/8 of the tetrahedral interstices in the close-packed metal atom lattice gives a structure comprising corner-linked TaO_6 octahedra and edge-shared CaO_8 distorted cubes. The basic repeating unit is a 6-Å thick slab parallel to (001) comprising a Ca_3Ta layer and a Ta_3Ca layer. Three such blocks, stacked along [001] in accord with the symmetry of space group $P3_121$, gives the trigonal weberite structure for $Ca_2Ta_2O_7$ (2). The short-hand notation for the 3-block trigonal structure is 3T.

From transmission electron microscopy and X-ray diffraction (XRD) studies on products from solid state syntheses, we showed that 3T $Ca_2Ta_2O_7$ transforms to a new polytype with monoclinic symmetry (2) at temperatures above 1400°C. The polytype is designated as 7M according to the above notation, having a $\sim \sqrt{3} \times a_{trig}$, $b \sim a_{trig}$ and $c \sim 7 \times 6$ Å. It was found that the 7M polytype was maintained in the niobia-doped samples up to 5 mole% substitution of $Ca_2Nb_2O_7$. However, at 10 mole% substitution, a monoclinic 5M polytype was formed. With an increase of the niobate component to 15 mole%, $Ca_2Nb_2O_7$ formed as a second phase. At 20 mole% doping the product from heating at 1500°C was almost pure $Ca_2Nb_2O_7$ with a trace only of the 5M polytype.

In this paper we report the determination and refinement of the structure for the 7M polytype of $Ca_2Ta_2O_7$ using

[1] To whom correspondence should be addressed.

0022-4596/01 $35.00

single-crystal XRD data and a refinement of the structure of the 7M polytype for $Ca_2Ta_{1.9}Nb_{0.1}O_7$ using powder neutron diffraction (ND) data. We also report the determination and refinement of the structure of the 5M polytype for $Ca_2Ta_{1.8}Nb_{0.2}O_7$ (stabilized by a trace amount of Mg), using powder XRD and ND data. In addition, we report dielectric measurements made on the 5M, 7M, and 3T (doped with $Nd_2Zr_2O_7$) polytypes over a wide frequency range, from 100 KHz to 10 GHz.

EXPERIMENTAL

Syntheses

Single crystals of 7M $Ca_2Ta_2O_7$ were grown in sealed platinum tubes using a 50 : 50 wt% mixture of prereacted tantalate with calcium vanadate ($Ca_2V_2O_7$). The tube was held at an initial temperature of 1450°C then slow cooled to 1150°C, held at this temperature for 400 h then removed from the furnace. The excess vanadate flux was washed away using dilute HCl. The crystals were in the form of small hexagonal platelets with sloping sides. The product comprised a mixture of 7M and 6M polytypes. We have previously reported the structure determination of the 6M polytype (2), which could only be prepared by flux growth—it did not form as a stable phase in the solid state syntheses. Electron microprobe analyses for the 7M polytype showed that the crystals were compositionally homogeneous, with 20.9 wt% CaO, 79.7 wt% Ta_2O_5, compared with calculated: 20.2% CaO, 79.8% Ta_2O_5 for $Ca_2Ta_2O_7$.

Polycrystalline, single-phase 7M $Ca_2Ta_{1.9}Nb_{0.1}O_7$ and 5M $Ca_2Ta_{1.8}Nb_{0.2}O_7$ were prepared from BDH AR grade $CaCO_3$ (99.9%), BDH laboratory grade Nb_2O_5 and Aldrich AR grade Ta_2O_5 (99.99%), weighed in the appropriate proportions, finely ground, pelletized, and then given a preliminary heat for 2 h at 900°C to decompose the carbonate. The samples were then heated to 1200°C for 2 h and to 1550°C for 16 h, with grinding and repelletization after each heating. Powder XRD patterns showed that both samples were single phases. The compositions were checked by X-ray fluorescence spectroscopy. The analysis of the 7M sample gave 76.8 wt% Ta_2O_5, 2.50 wt% Nb_2O_5, and 20.6 wt% CaO, compared with calculated values of 77.0% Ta_2O_5, 2.44% Nb_2O_5, and 20.6% CaO for $Ca_2Ta_{1.9}Nb_{0.1}O_7$. The analysis of the 5M sample gave 74.1 wt% Ta_2O_5, 5.02 wt%, Nb_2O_5 and 21.0 wt% CaO, compared with calculated values of 74.1% Ta_2O_5, 4.95% Nb_2O_5, and 20.9% CaO for $Ca_2Ta_{1.8}Nb_{0.2}O_7$.

Single-phase 3T $Ca_{1.6}Nd_{0.4}Ta_{1.6}Zr_{0.4}O_7$ was prepared by using the appropriate mixtures of $CaCO_3$, Ta_2O_5, Nd_2O_3, and ZrO_2 and by following the same heating conditions as described for the niobia-doped 5M and 7M polytypes, with the final heating at 1550°C. The $Nd_2Zr_2O_7$-doped sample has the 3T polytype structure, which is adopted by $Ca_2Ta_2O_7$ at or below 1400°C. The doping allowed the 3T structure to be stabilized to 1550°C so it could be prepared for dielectric measurements using the same sintering conditions as for the 5M and 7M polytypes.

Diffraction Studies

Electron diffraction/microscopy studies were made using a Philips 430 transmission electron microscope (TEM) operated at 300 kV. Crystals were crushed in an agate mortar and dispersed on a holey carbon grid for study.

Single-crystal intensity data for 7M $Ca_2Ta_2O_7$ were collected using a Nonius Kappa diffractometer employing a CCD area detector. To minimize absorption effects, a small hexagonal platelet was selected, which was 0.03 mm thick and had maximum basal plane dimension of 0.06 mm. A full sphere of intensity data was collected at 293 K using a combination of ϕ and ω° scans, at 0.5° steps and with counting times of 32 s per scan. The crystal-to-detector distance was 65 mm. The CCD intensity data were corrected numerically for absorption ($\mu = 40.3\ mm^{-1}$) using Nonius software and converted to F^2s, which were used with SHELXL (5) for the structure determination and refinements. Further details are given in Table 1.

Powder specimens were prepared in the form of sintered 10×50 mm cylinders. They were contained in vanadium cans for the ND intensity data sets, which were collected using the 32-counter powder diffractometer at the reactor of the National Institute of Standards and Technology, Washington. Data were collected at room temperature, at 0.05° steps in the angular range 3 to 150° (2θ) using a monochromatic beam of wavelength 1.540(1) Å.

Step-scan powder XRD patterns were collected on ball-milled samples using a Philips 1050 diffractometer, employing a long fine-focus copper tube operated at 40 kV and 40 mA. The diffractometer was configurated with a 1°

TABLE 1
Crystallographic Data for 7M $Ca_2Ta_2O_7$

Crystal data	
$Ca_2Ta_2O_7$, Mf = 554.06	$a = 12.726(1)$, $b = 7.380(1)$,
Monoclinic, $C2$	$c = 42.538(1)$ Å, $\beta = 95.77(1)°$, $Z = 28$
Hexagonal plate, 0.06×0.06×0.03 mm	$D_x = 6.48\ Mg\ m^{-3}$, $\mu = 40.3\ mm^{-1}$
Intensity measurements	
Nonius Kappa CCD diffractometer	ϕ and ω scans, $2\theta_{max} = 56°$
Mo$K\alpha$ radiation, $t = 293$ K	$h = -16 \rightarrow 16$, $k = -8 \rightarrow 8$,
	$l = -55 \rightarrow 55$
Absorption correction: numerical face	13,351 measured reflections
indexed. $T_{min} = 0.15$, $T_{max} = 0.33$	7965 independent reflections
$R_{int} = 0.031$	6535 reflections with $F > 4\sigma(F)$
Refinement	
Refinement of F^2, 454 parameters	$R(F) = 0.028$ for $F \gg 4\sigma(F)$
$\Delta\rho_{max} = 1.79\ eÅ^{-3}$	$R(F) = 0.040$ for all data
$\Delta\rho_{min} = -2.14\ eÅ^{-3}$	$wR(F^2) = 0.13$ for all data, $S = 0.71$

divergent slit, 0.2 mm receiving slit, 1° scatter slit, incident and diffracted beam Soller slits, and a diffracted-beam graphite monochromator.

Least-squares refinements were made using the Rietveld program CSRIET/SR5, a local modification of the code by Hill and Howard (6) and Wiles and Young (7). A Voigt peak shape function was employed, together with a three-term full-width at half-maximum function (8) and a four-parameter polynomial for the background.

Structure Determinations and Refinements

7M $Ca_2Ta_2O_7$. The precession method was used to check the quality of single crystals and to establish the unit cell dimensions and symmetry. The monoclinic cell parameters were subsequently refined using powder XRD data, giving the values reported in Table 1. The systematic absences in precession photos were consistent with the space groups *C*2/*m*, *C*2, or *Cm*.

The establishment of a structural model for the 7M polytype of $Ca_2Ta_2O_7$ was assisted by the analysis of high-resolution TEM images projected along the pseudo-trigonal 7.35 Å axes. A [110] zone axis diffraction pattern is shown in Fig. 1c, together with the associated low-resolution, Fig. 1a, and high-resolution, Fig. 1b, images. The low-resolution image shows that the 7M polytype periodicity is maintained over extended regions.

TEM images show distinctive herring-bone patterns of rows of dark (or light, depending on the crystal thickness and defocus) spots which could be interpreted in terms of

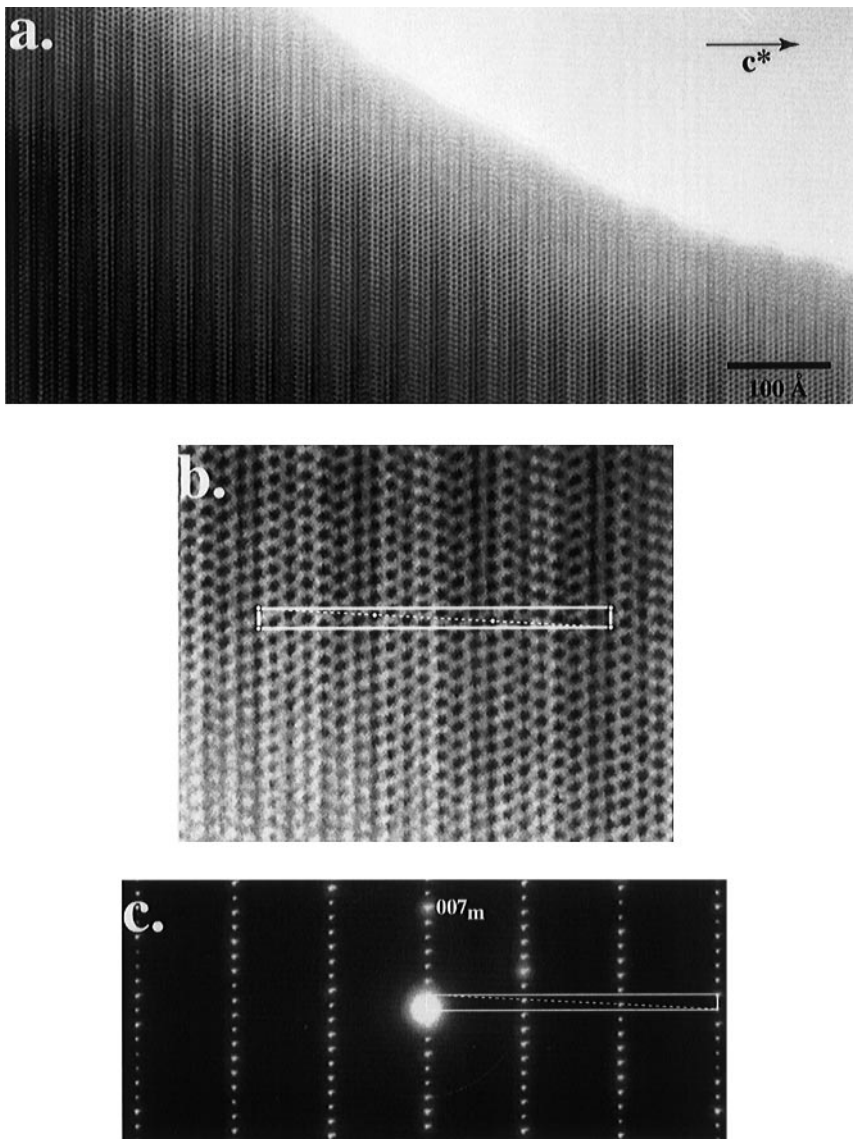

FIG. 1. (a) Low-resolution TEM image for 7M-$Ca_2Ta_2O_7$ viewed along [110], (b) high-resolution image, pseudo-trigonal cell outlined, (c) corresponding [110] zone electron diffraction pattern, c* axis is vertical.

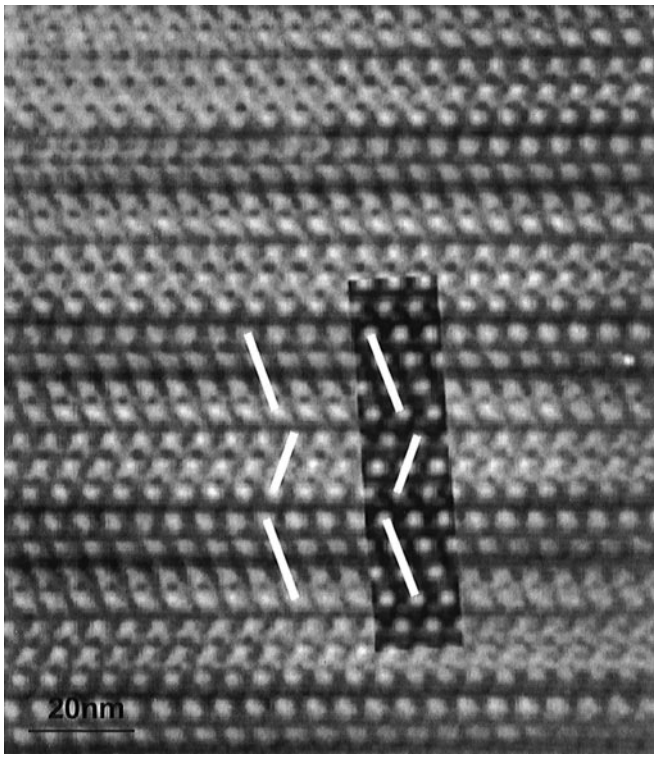

FIG. 2. [110] TEM image for 7M-$Ca_2Ta_2O_7$ taken at a defocus of 70 nm, near the Scherzer condition. The inset is a simulated image of the structure, calculated for an 8-mm^{-1} aperture and a crystal thickness of 20 nm. The herring-bone pattern of rows of projected metal atoms forming 3-blocks and 4-blocks is indicated by the white lines.

the projected chains of metal atoms. We previously reported (2) how this interpretation was used to establish the structural model for 6M $Ca_2Ta_2O_7$. The herring-bone patterns are outlined for the 7M polytype in Fig. 2, taken at a defocus near the Scherzer condition. They correspond to an alternation of 3-blocks and 4-blocks, where a block comprises an adjacent pair of Ca_3Ta and Ta_3Ca fluorite-type metal atom layers as explained in the Introduction. The TEM images show that adjacent blocks are offset due to a change in the stacking sequence of the (001) metal atom layers from cubic stacking to hexagonal stacking at the interface between the blocks. By analogy with the 6M polytype structure, the hexagonal-stacked metal atom layers were considered to have the composition Ta_3Ca. The HRTEM image for the 7M polytype is consistent with a metal atom layer stacking sequence given by *cccchccccccch* ... .

The intralayer ordering of Ca and Ta in the Ca_3Ta and Ta_3Ca layers was determined by the testing of all possible combinations using low angle powder XRD data. The dominance of the Ta and Ca contributions to the diffraction peaks means that the peak intensities are closely reproduced by considering the metal atoms only, as shown in Fig. 3a. By restricting the powder pattern to the low angle region, the calculated intensities were not sensitive to small metal atom displacements and so the ideal coordinates could be used, based on a close-packed metal atom array. The use of powder XRD data in this way gave a rapid, sensitive, visual screening of the different possible Ca/Ta orderings. In considering different possible ordering schemes, the three possible space groups, $C2$, Cm, and $C2/m$ were tested. A good match to the observed XRD pattern could only be obtained using the space group $C2$. Refinement of this metal atom ordering model using the single-crystal data gave an agreement factor, $R1 = 0.13$.

The positions of the oxygen atoms were located in Fourier and difference Fourier maps. Refinement of all atomic coordinates and individual atomic displacement parameters (anisotropic for the metal atoms and isotropic for the oxygen atoms) resulted in convergence at the R values given in Table 1. The final refined structural parameters were input to the program Platon (9) to test if the symmetry was higher than $C2$. No higher symmetry (in particular $C2/m$) was found. The refined coordinates and isotropic displacement parameters for 7M $Ca_2Ta_2O_7$ are given in Table 2. Tables of structure factors and anisotropic displacement parameters for the metal atoms are available from the authors. The refined structure was used to generate a simulated TEM image, projected along [110]. The simulated image is inset in the corresponding experimental image in Fig. 2. A good match was obtained using an 8 mm^{-1} aperture, a crystal thickness of 20 nm, and a 70 mm defocus (near Scherzer condition for the Philips 430 TEM operated at 300 kV).

7M $Ca_2Ta_{1.9}Nb_{0.1}O_7$. The refined structure for 7M $Ca_2Ta_2O_7$ was used as a starting model for the refinement of the powder ND data for $Ca_2Ta_{1.9}Nb_{0.1}O_7$. A refinement of all metal and oxygen atom coordinates and group isotropic thermal parameters for calcium, tantalum, and oxygen atoms proceeded smoothly and converged at the agreement values given in Table 3. In Table 3, the refined cell parameters are from refinement of XRD data, where the wavelength is more accurately known. Using the powder ND data it was not possible to determine if the niobium was ordered into specific metal atom sites. In the refinement the niobium atoms were statistically distributed over all the metal atom sites. The refined parameters are compared with those for $Ca_2Ta_2O_7$ in Table 2.

5M $Ca_2Ta_{1.8}Nb_{0.2}O_7$. The powder XRD pattern for $Ca_2Ta_{1.8}Nb_{0.2}O_7$ could be fully indexed using a C-centered monoclinic cell which was refined to give the parameters $a = 12.7528\,(4)$, $b = 7.3492\,(2)$, $c = 30.2442\,(8)$ Å, $\beta = 94.245\,(2)^\circ$. These parameters are almost the same as those for the Sm/Ti-doped 5M polytype, $Ca_{1.8}Ta_{1.8}Sm_{0.24}Ti_{0.17}O_7$ (3). We have recently determined the structure of the Sm/Ti-doped phase using single-crystal XRD methods and have

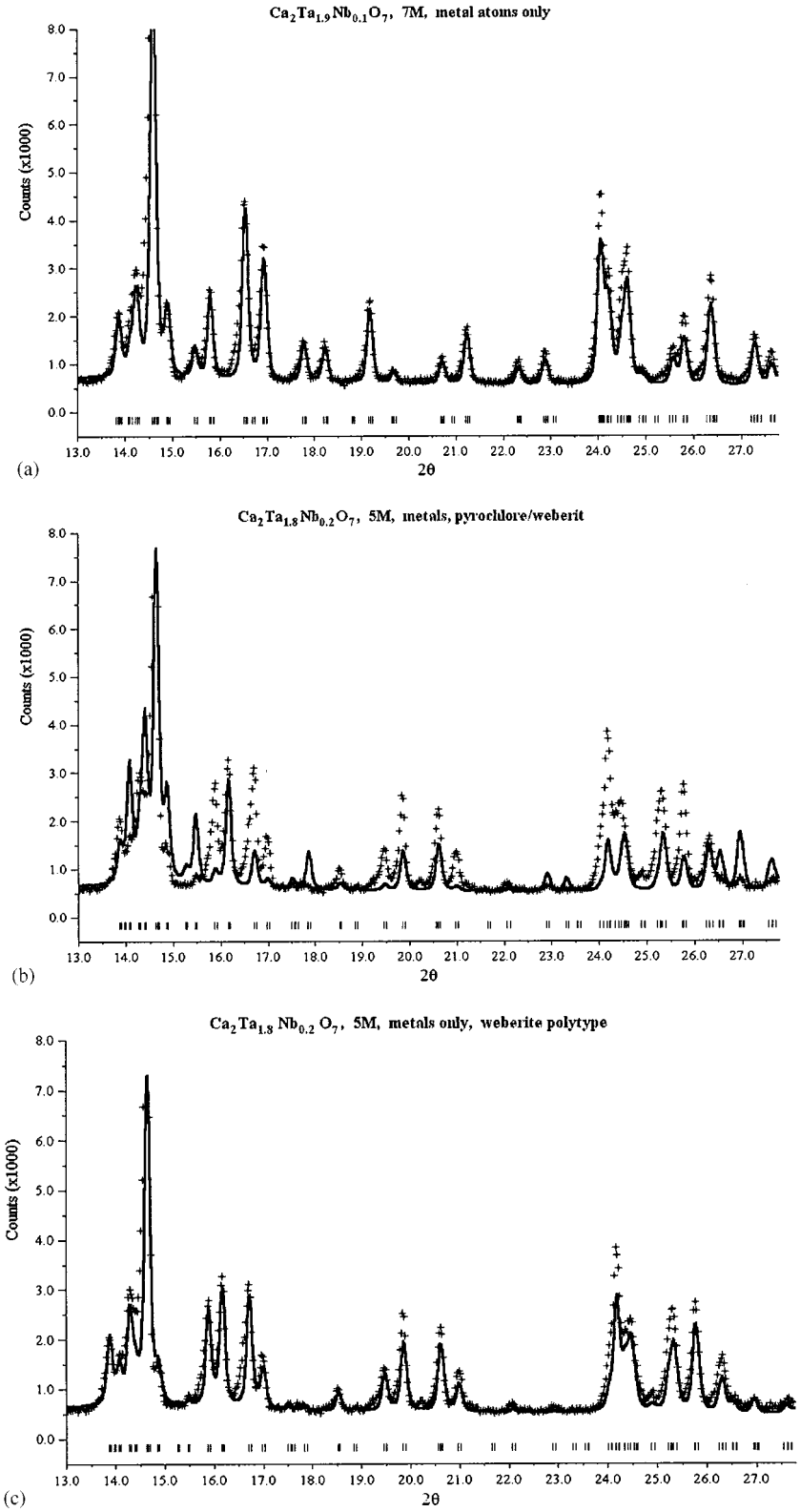

FIG. 3. X-ray diffractograms for (a) 7M-$Ca_2Ta_{1.9}Nb_{0.1}O_7$, (b) and (c) 5M-$Ca_2Ta_{1.8}Nb_{0.2}O_7$. Solid line is calculated and crosses are observed data. Bragg reflections are marked.

TABLE 2
Refined Structure Parameters for 7M $Ca_2Ta_2O_7$ and 7M $Ca_2Ta_{1.9}Nb_{0.1}O_7$

	7M $Ca_2Ta_2O_7$ Single crystal XRD refinement				7M $Ca_2Ta_{1.9}Nb_{0.1}O_7$ Powder ND refinement*		
	x	y	z	U, Å^2	x	y	z
Ta(1)	0	0.0289(2)	0	0.007(1)	0	0.029(5)	0
Ca(1)	0	0.490(1)	0	0.010(1)	0	0.509(7)	0
Ca(11)	0.2531(3)	0.2322(9)	− 0.0023(1)	0.010(1)	0.262(3)	0.213(4)	− 0.0027(7)
Ta(21)	0.1894(1)	− 0.0020(2)	0.0717(1)	0.006(1)	0.187(2)	0.002(4)	0.0714(4)
Ta(22)	0.1892(1)	0.4975(2)	0.0707(1)	0.006(1)	0.190(2)	0.502(4)	0.0707(6)
Ta(2)	0.4394(1)	0.2509(2)	0.0694(1)	0.006(1)	0.439(2)	0.246(4)	0.0693(5)
Ca(2)	0.4357(3)	0.758(1)	0.0731(1)	0.015(1)	0.440(3)	0.746(5)	0.0734(7)
Ca(31)	0.1275(3)	0.2657(9)	0.1409(1)	0.015(1)	0.134(3)	0.274(5)	0.1428(7)
Ca(32)	0.1274(3)	0.7607(9)	0.1422(1)	0.013(1)	0.125(3)	0.759(5)	0.1413(8)
Ta(3)	0.3826(1)	0.0070(2)	0.1441(1)	0.006(1)	0.385(2)	0.001(4)	0.1449(4)
Ca(3)	0.3763(3)	0.505(1)	0.1413(1)	0.016(1)	0.379(3)	0.507(6)	0.1411(6)
Ta(41)	0.0618(1)	0.0186(1)	0.2112(1)	0.006(1)	0.061(2)	0.018(4)	0.2113(4)
Ta(42)	0.0659(1)	0.5184(1)	0.2184(1)	0.006(1)	0.069(2)	0.517(4)	0.2180(5)
Ca(4)	0.3162(2)	0.257(1)	0.2125(1)	0.010(1)	0.318(3)	0.253(5)	0.2128(7)
Ta(4)	0.3140(1)	0.7660(2)	0.2161(1)	0.006(1)	0.315(2)	0.767(4)	0.2157(5)
Ca(51)	0.1764(3)	0.2709(9)	0.2878(1)	0.013(1)	0.182(3)	0.262(5)	0.2890(6)
Ca(52)	0.1858(3)	0.7707(9)	0.2889(1)	0.022(1)	0.180(3)	0.761(4)	0.2882(7)
Ca(5)	0.4263(2)	0.0161(9)	0.2858(1)	0.011(1)	0.421(3)	0.020(5)	0.2838(6)
Ta(5)	0.4285(1)	0.4922(2)	0.2841(1)	0.007(1)	0.429(2)	0.499(4)	0.2842(4)
Ta(6)	0.0361(1)	0.2617(2)	0.3559(1)	0.006(1)	0.035(2)	0.258(4)	0.3569(5)
Ca(6)	0.0329(3)	0.767(1)	0.3564(1)	0.017(1)	0.029(3)	0.759(5)	0.3561(8)
Ta(61)	0.2888(1)	0.0110(2)	0.3580(1)	0.006(1)	0.286(2)	0.013(4)	0.3577(5)
Ta(62)	0.2874(1)	0.5130(2)	0.3590(1)	0.006(1)	0.287(2)	0.516(4)	0.3583(4)
Ca(7)	0.1521(3)	0.0076(9)	0.4274(1)	0.014(1)	0.152(2)	0.006(6)	0.4271(6)
Ta(7)	0.1305(1)	0.5241(2)	0.4284(1)	0.007(1)	0.132(2)	0.514(6)	0.4287(8)
Ca(71)	0.3957(3)	0.257(1)	0.4284(1)	0.012(1)	0.397(3)	0.258(5)	0.4260(7)
Ca(72)	0.3989(3)	0.7437(9)	0.4307(1)	0.012(1)	0.394(3)	0.757(5)	0.4308(7)
Ta(8)	0	0.0051(2)	0.5	0.006(1)	0	0.008(6)	0.5
Ca(8)	0	0.507(2)	0.5	0.020(2)	0	0.492(7)	0.5
Ta(81)	0.2518(1)	0.7579(2)	0.5018(1)	0.006(1)	0.251(3)	0.753(6)	0.5010(8)
O(1)	0.1364(7)	0.005(2)	0.0267(2)	0.008(2)	0.136(2)	− 0.009(5)	0.0246(7)
O(2)	0.1834(8)	0.464(2)	0.0248(3)	0.009(2)	0.180(3)	0.495(5)	0.0225(7)
O(3)	0.4339(8)	0.713(2)	0.0228(3)	0.007(2)	0.449(3)	0.714(5)	0.0224(9)
O(4)	0.4397(8)	0.313(2)	0.0247(3)	0.009(2)	0.441(3)	0.314(5)	0.0263(8)
O(5)	0.3255(8)	0.081(2)	0.0575(3)	0.011(2)	0.324(3)	0.074(4)	0.0602(7)
O(6)	0.0361(8)	0.547(2)	0.0629(3)	0.008(2)	0.033(3)	0.539(5)	0.0634(6)
O(7)	0.7377(7)	0.252(2)	0.0633(2)	0.007(2)	0.747(2)	0.245(5)	0.0654(8)
O(8)	0.1399(8)	0.249(2)	0.0788(2)	0.007(2)	0.144(2)	0.253(6)	0.0771(7)
O(9)	0.3437(7)	0.444(2)	0.0777(2)	0.003(2)	0.339(3)	0.447(5)	0.0788(7)
O(10)	0.5546(9)	0.416(2)	0.0843(3)	0.012(2)	0.557(3)	0.412(4)	0.0865(7)
O(11)	0.9437(8)	0.678(2)	0.1151(3)	0.009(2)	0.949(3)	0.678(4)	0.1152(8)
O(12	0.1969(7)	0.531(2)	0.1171(2)	0.009(2)	0.200(3)	0.531(5)	0.1189(7)
O(13)	0.2466(8)	0.982(2)	0.1156(3)	0.017(2)	0.249(2)	0.977(5)	0.1134(7)
O(14)	0.4415(8)	0.790(2)	0.1250(3)	0.012(2)	0.441(3)	0.787(5)	0.1249(6)
O(15)	0.3135(8)	0.223(2)	0.1601(2)	0.007(2)	0.312(3)	0.232(5)	0.1612(7)
O(16)	0.0627(7)	0.002(2)	0.1662(2)	0.007(2)	0.057(3)	0.032(5)	0.1654(6)
O(17)	0.0176(7)	0.514(2)	0.1706(2)	0.012(2)	0.013(2)	0.523(5)	0.1706(7)
O(18)	0.3054(7)	0.841(2)	0.1709(3)	0.006(2)	0.308(3)	0.842(5)	0.1704(8)
O(19)	0.7046(8)	0.091(2)	0.2053(2)	0.010(2)	0.707(3)	0.091(3)	0.2070(8)
O(20)	0.4074(8)	0.569(2)	0.2035(3)	0.009(2)	0.411(3)	0.558(4)	0.2057(6)
O(21)	0.5185(8)	0.272(2)	0.2163(3)	0.009(2)	0.516(2)	0.271(5)	0.2121(7)
O(22)	0.6182(8)	0.771(2)	0.2124(2)	0.008(2)	0.618(2)	0.767(5)	0.2146(7)
O(23)	0.2080(8)	0.948(2)	0.2259(3)	0.011(2)	0.222(3)	0.946(4)	0.2255(7)
O(24)	0.4197(9)	0.963(2)	0.2262(3)	0.017(3)	0.414(3)	0.979(5)	0.2257(6)
O(25)	0.0440(8)	0.052(2)	0.2583(3)	0.010(2)	0.045(3)	0.055(4)	0.2593(8)

TABLE 2—*Continued*

	7M $Ca_2Ta_2O_7$ Single crystal XRD refinement				7M $Ca_2Ta_{1.9}Nb_{0.1}O_7$ Powder ND refinement*		
	x	*y*	*z*	*U*, Å^2	*x*	*y*	*z*
O(26)	0.3389(9)	0.707(2)	0.2612(3)	0.011(2)	0.345(3)	0.705(5)	0.2610(9)
O(27)	0.3400(8)	0.312(2)	0.2637(2)	0.008(2)	0.337(3)	0.299(5)	0.2644(8)
O(28)	0.6000(7)	0.024(2)	0.2633(2)	0.010(2)	0.596(3)	0.038(5)	0.2628(8)
O(29)	0.5145(8)	0.306(2)	0.3046(3)	0.011(2)	0.508(3)	0.302(4)	0.3060(7)
O(30)	0.0022(7)	0.203(2)	0.3122(2)	0.005(2)	− 0.004(3)	0.207(5)	0.3106(8)
O(31)	0.8185(8)	0.010(2)	0.3143(2)	0.012(2)	0.807(3)	0.018(5)	0.3127(7)
O(32)	0.7664(7)	0.532(2)	0.3112(2)	0.006(2)	0.771(3)	0.554(4)	0.3109(7)
O(33)	0.4405(9)	0.973(2)	0.3511(3)	0.014(3)	0.436(3)	− 0.037(4)	0.3517(7)
O(34)	0.6449(7)	0.927(2)	0.3429(2)	0.003(2)	0.642(3)	− 0.066(4)	0.3445(7)
O(35)	0.2345(8)	0.761(2)	0.3513(2)	0.008(2)	0.234(2)	0.757(6)	0.3471(7)
O(36)	0.1408(8)	0.063(2)	0.3629(3)	0.011(2)	0.145(3)	0.071(5)	0.3625(7)
O(37)	0.8397(7)	0.764(2)	0.3654(2)	0.008(2)	0.841(3)	0.765(5)	0.3655(7)
O(38)	0.4326(8)	0.593(2)	0.3720(3)	0.011(2)	0.423(3)	0.599(4)	0.3694(8)
O(39)	0.2652(7)	0.522(2)	0.4038(2)	0.008(2)	0.267(2)	0.522(6)	0.4034(8)
O(40)	0.0701(8)	0.730(2)	0.4066(3)	0.011(2)	0.065(3)	0.724(5)	0.4053(9)
O(41)	0.8111(7)	0.481(2)	0.4040(2)	0.005(2)	0.813(3)	0.491(5)	0.4036(8)
O(42)	0.0728(9)	0.326(2)	0.4020(3)	0.013(2)	0.076(3)	0.319(5)	0.4023(9)
O(43)	0.2135(8)	0.309(2)	0.4537(3)	0.009(2)	0.211(3)	0.305(5)	0.4536(9)
O(44)	0.5062(7)	0.999(2)	0.4492(2)	0.008(2)	0.504(3)	0.003(5)	0.4510(6)
O(45)	0.7142(8)	0.199(2)	0.4563(3)	0.007(2)	0.714(3)	0.191(4)	0.4557(8)
O(46)	0.0030(7)	0.007(2)	0.4538(2)	0.010(2)	− 0.006(3)	0.025(5)	0.4541(7)
O(47)	0.2726(7)	0.003(2)	0.4864(2)	0.011(2)	0.274(3)	0.006(5)	0.4861(6)
O(48)	0.1004(9)	0.803(2)	0.5069(3)	0.009(3)	0.100(3)	0.811(5)	0.5078(9)
O(49)	0.1031(8)	0.210(2)	0.5064(3)	0.007(2)	0.098(3)	0.214(5)	0.5078(8)

* B(Ta) = 0.39 (3), B(Ca) = 0.80 (4), B(Ox) = 1.04 (1) Å^2 for 7M $Ca_2Ta_{1.9}Nb_{0.1}O_7$.

shown that it can be described as an ordered intergrowth of weberite-type and pyrochlore-type blocks (3). However, when the metal atom ordering in the Sm/Ti-doped 5M polytype was used in the calculation of the power XRD pattern, a poor agreement with the observed pattern for $Ca_2Ta_{1.8}Nb_{0.2}O_7$ was obtained as shown in Fig. 3b.

TABLE 3
Crystallographic Data for 7M $Ca_2Ta_{1.9}Nb_{0.1}O_7$ and 5M $Ca_2Ta_{1.8}Nb_{0.2}O_7$

	7M $Ca_2Ta_{1.9}Nb_{0.1}O_7$	5M $Ca_2Ta_{1.8}Nb_{0.2}O_7$
Cell parameters*		
a (Å)	12.7170 (6)	12.7528 (4)
b (Å)	7.3728 (3)	7.3492(2)
c (Å)	42.464 (2)	30.2442(8)
β (°)	95.755 (5)	94.245 (2)
Space group	*C*2	*C*2
Z	28	20
Intensity data collect	Powder ND	Powder ND
Wavelength (Å)	1.5402	1.5402
2θ range refined	3–140°	3–140°
No. parameters refined	248	181
Total no. reflections	4217	3006
Rwp	0.053	0.057
R_B	0.022	0.027
GOF.	1.45	1.90

* From refinement of powder XRD data.

Using the low-angle powder XRD pattern for screening, the metal atom ordering of the Sm/Ti-doped tantalate polytype was systematically varied until good agreement with the observed pattern for $Ca_2Ta_{1.8}Nb_{0.2}O_7$ was obtained. The best match to the observed pattern, shown in Fig. 3c, was obtained when the Ca atom and a Ta atom were interchanged in the central Ta_3Ca layer of the pyrochlore block. The same space group, *C*2, was maintained. The new arrangement of metal atoms was input to a Rietveld refinement using powder neutron data. The new oxygen positions around the interchanged metal atoms and around the metal atoms with which they share anions were obtained from difference Fourier maps. When all the displaced oxygen atoms were located the refinement progressed smoothly, and converged at $R_{wp} = 0.057$, $R_B = 0.027$ for refinement of all coordinates and group isotropic temperature parameters for Ca, Ta, and O. As we found for the 7M polytype, it was not possible using the powder diffraction data to determine if the niobium was ordered into specific metal atom sites. In the refinement the niobium atoms were statistically distributed over all the metal atom sites. The final refined structural parameters were input to the program Platon (9) to test if the symmetry was higher than *C*2. No higher

TABLE 4
Refined Structure Parameters* for 5M $Ca_2Ta_{1.8}Nb_{0.2}O_7$

	x	*y*	*z*
Ta(1)	0	0.028(4)	0
Ca(11)	0	0.497(7)	0
Ca(12)	0.247(2)	0.226(3)	− 0.0034(8)
Ta(2)	0.184(2)	− 0.010(3)	0.1009(7)
Ta(21)	0.182(2)	0.489(3)	0.1000(7)
Ca(22)	0.435(1)	0.249(4)	0.0980(6)
Ca(23)	0.422(2)	0.748(5)	0.0998(8)
Ta(3)	0.372(2)	0.000(3)	0.2030(5)
Ca(31)	0.365(2)	0.504(5)	0.1949(7)
Ca(32)	0.601(2)	0.255(4)	0.1972(7)
Ca(33)	0.628(2)	0.745(5)	0.2021(7)
Ca(4)	0.549(2)	0.003(4)	0.2994(8)
Ta(41)	0.553(2)	0.502(3)	0.2964(6)
Ta(42)	0.805(2)	0.256(3)	0.3048(5)
Ta(43)	0.800(2)	0.749(4)	0.3000(6)
Ca(5)	0.398(2)	0.013(4)	0.4011(7)
Ca(51)	0.394(2)	0.509(5)	0.4050(7)
Ca(52)	0.653(2)	0.263(4)	0.4028(7)
Ta(53)	0.641(2)	0.758(3)	0.3966(5)
Ta(6)	0.255(2)	− 0.007(3)	0.4969(5)
Ta(61)	0.5	0.250(5)	0.5
Ca(62)	0.5	0.767(5)	0.5
O(1)	0.129(2)	− 0.005(4)	0.0397(7)
O(2)	0.420(2)	0.708(3)	0.0311(7)
O(3)	0.440(2)	0.301(3)	0.0352(7)
O(4)	0.172(2)	0.458(3)	0.0337(6)
O(5)	0.531(2)	0.039(4)	0.0898(6)
O(6)	0.233(2)	0.739(4)	0.0962(6)
O(7)	0.822(2)	0.565(3)	0.0822(7)
O(8)	0.337(2)	0.460(3)	0.1063(6)
O(9)	0.628(2)	0.741(4)	0.1085(6)
O(10)	0.545(2)	0.415(3)	0.1195(7)
O(11)	0.427(2)	0.784(3)	0.1748(7)
O(12)	0.735(2)	0.497(4)	0.1635(6)
O(13)	0.420(2)	0.185(3)	0.1613(7)
O(14)	0.679(2)	0.008(4)	0.1643(6)
O(15)	0.520(2)	0.013(4)	0.2282(6)
O(16)	0.022(2)	− 0.017(4)	0.2319(6)
O(17)	0.290(2)	0.819(3)	0.2377(7)
O(18)	0.321(2)	0.210(3)	0.2345(7)
O(19)	0.267(2)	0.500(4)	0.2845(6)
O(20)	0.146(2)	0.205(3)	0.2834(6)
O(21)	0.149(2)	0.796(3)	0.3008(7)
O(22)	0.452(2)	0.699(3)	0.3024(7)
O(23)	0.445(2)	0.330(3)	0.3143(7)
O(24)	0.356(2)	0.006(4)	0.3159(6)
O(25)	0.275(2)	0.273(4)	0.3639(7)
O(26)	0.089(2)	0.043(4)	0.3620(7)
O(27)	0.807(2)	0.242(4)	0.3696(6)
O(28)	0.073(2)	0.465(3)	0.3700(7)
O(29)	0.011(2)	0.239(4)	0.4302(6)
O(30)	0.000(2)	0.755(4)	0.4318(7)
O(31)	0.716(2)	0.551(3)	0.4352(7)
O(32)	0.218(2)	0.431(3)	0.4399(7)
O(33)	0.098(2)	0.547(3)	0.5092(8)
O(34)	0.902(2)	0.960(4)	0.4946(7)
O(35)	0.224(2)	0.243(4)	0.5202(6)

* B(Ta) = 0.39(4), B(Ca) = 1.10(8), B(Ox) = 0.91 (2) Å^2.

symmetry was found. The refinement details are given in Table 3. The refined structural parameters are reported in Table 4.

Dielectric Measurements

The complex permittivity ε^* was determined in the 100 kHz–10 GHz frequency range by the measurement of the reflection coefficient Γ^* of a cylindrical sample ending a coaxial line in the APC7 standard. Measurements were performed using three network analyzers (HP4192A, HP4191A, and AW37200A) on samples measuring 7 mm in diameter and 2–3 mm in thickness. For such thicknesses and above 100 MHz, the electromagnetic configuration can no longer be approximated by a lumped circuit and the wave propagation inside the sample must be considered. In our geometry—a junction between a coaxial and a cylindrical waveguide—an exact coupled-mode theory (10) can be used to compute the complex admittance $Y^* = Y_0 (1 - \Gamma^*)/(1 + \Gamma^*)$ as a function of ε^* ($Y_0 = 20$ mS is the characteristic admittance of the line).

RESULTS AND DISCUSSION

7M $Ca_2Ta_2O_7$ and $Ca_2Ta_{1.9}Nb_{0.1}O_7$ Structures

A projection of the 7M polytype structure along the *b* axis is shown in Fig. 4. The Ta-centered octahedra are labeled as in Table 2. The calcium atoms are shown by the filled circles. A significant difference exists between the metal atom arrangements in the 7M polytype and in 3T $Ca_2Ta_{2-x}Nb_xO_7$, which is the stable polytype at temperatures of 1400°C and lower. The metal atoms in the 3T structure are in *fcc* close packing as in the fluorite structure, whereas in the 7M polytype the cubic stacking of the (001) metal atom layers is modified by the incorporation of hexagonal-stacked layers of metals. The *h*-stacked metal atom layers have composition Ta_3Ca. The TaO_6 octahedra in this layer are shown by dark shading in Fig. 4. The stacking sequence of metal atom layers in the 7M polytype in *hccccchccccccch*.... The basic repeating unit is a 6 Å slab parallel to (001) comprising a Ca_3Ta layer and a Ta_3Ca layer. In the 7M polytype the *h*-stacked Ta_3Ca layers divide the structure into two blocks of *c*-stacked layers, which contain 3 and 4 repeating units and can be thus designated as 3M and 4M blocks. The 3M and 4M block features are evident in TEM images as shown by the white markers in Fig. 2.

The connectivity of the octahedra in the *h*-Ta_3Ca layer, as in the *c*-Ta_3Ca layers, is of the hexagonal tungsten bronze (HTB) type (11). In the calcium tantalate polytypes, the HTB octahedra in the Ta_3Ca layers are interconnected via corner sharing with isolated octahedra in the intervening Ca_3Ta layers. Only four of the vertices of the isolated octahedra are involved in the interlayer connectivity, as occurs also in the different weberite polytypes (12).

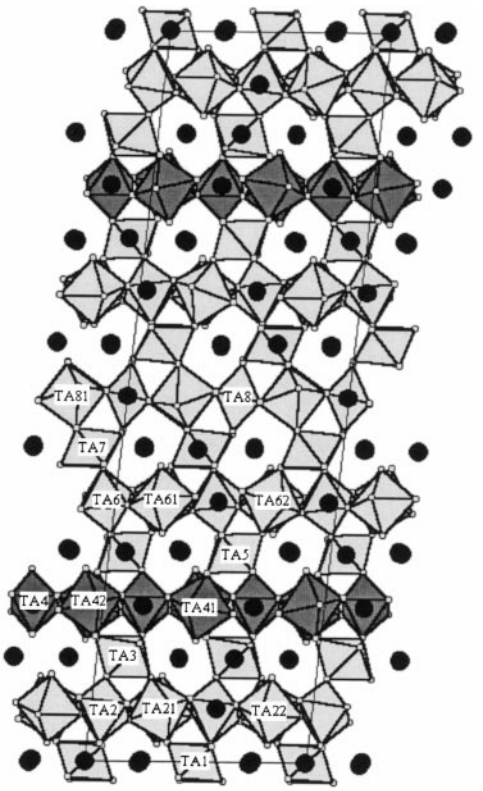

FIG. 4. [010] Projection of structure of 7M-$Ca_2Ta_{1.9}Nb_{0.1}O_7$. Dark shaded octahedra correspond to hexagonal-stacked Ta_3Ca layers. The unit cell outline is shown, *c* axis is vertical, Ta atoms are labelled.

A distinction can be made between the relative location of the two nonbridging vertices of the isolated octahedra in the Ca_3Ta layers. These can be in a *cis* or *trans* configuration, and the different polytypes are distinguished by the sequence of *cis* and *trans* octahedra in the Ca_3Ta layers. In the 7M polytype the sequence of Ca_3Ta layers is *trans* –*cis*–*trans*–*cis*–*cis*–*cis*–*cis*–...., where the Ta(3)–O_6 octahedra have the *trans* form and the Ta(1)O_6, Ta(5)O_6 and Ta(7)O_6 octahedra have the *cis* form. A description of the stacking sequence of all 14 metal atom layers in the 7M polytype is given by:

3M block: *h*-Ta_3Ca–*trans*-Ca_3Ta–*c*-Ta_3Ca–*cis*-Ca_3Ta–*c*-Ta_3Ca–*trans*-Ca_3Ta–*h*-Ta_3Ca–
4M block: *h*-Ta_3Ca–3(*cis*-Ca_3Ta–*c*-Ta_3Ca)–*cis*-Ca_3Ta–*h*-Ta_3Ca–,

where the *h*-stacked and *c*-stacked Ta_3Ca layers are identified as are the *trans*- and *cis*-terminal oxygens of the Ta atoms in the Ca_3Ta layers.

Table 5 gives the ranges of polyhedral Ta–O and Ca–O distances in 7M $Ca_2Ta_2O_7$, as well as the mean distances for each polyhedron. In the case of the Ca-centered polyhedra, the coordination is given as 8, 7 + 1, or 6 + 2 on the basis of relatively large increases (0.2–0.4 Å) in the distances to the seventh and eighth oxygen atoms for some calcium atoms.

The average Ta–O distances are in a relatively narrow range, 1.96 to 2.00 Å, and are typical of mean distances for tantalates. The longest mean distances and the largest spread of distances are associated with Ta(1), Ta(5), and Ta(7). These correspond to the isolated octahedra in the *cis*-Ca_3Ta layers. In each case the distortion of the octahedron results from displacement of the Ta atom toward the octahedral edge comprising the two nonbridging oxygen atoms in *cis*-configuration. These terminal oxygen atoms coordinate to only one Ta atom and three Ca atoms and so they are formally undersaturated. Their valence requirements are satisfied by a displacement of the Ta atom toward them. For example, in the case of Ta(1), the nonbridging oxygens are O(3). The two Ta(1)–O(3) distances are 1.91 Å, compared to two Ta(1)–O(1) distances of 1.98 Å and two Ta(1)–O(4) distances of 2.10 Å. The displacement of the Ta atom in each case is along the direction of one of the pseudotrigonal chains of alternating Ca and Ta atoms in the *cis*-Ca_3Ta layers. This results in an alternation of long and short Ca–Ta distances along the chain. In the case of Ta(1), the Ta(1)–Ca(1) distances are 3.40 and 3.98 Å. This represents a large distortion from close-packing of the metal atoms as in fluorite, where all the distances would be equal at $\sim$ 3.7 Å. We have reported similar distortions associated with the *cis*-Ca_3Ta layers in 5M and 6T polytypes of Sm, Ti-doped $Ca_2Ta_2O_7$ (3) and the reader is referred to this reference for further discussion and structural diagrams showing the *cis*-octahedra.

The Ta(4), Ta(41), and Ta(42) atoms form the *h*-stacked Ta_3Ca layer. This is a pseudo mirror plane for the metal atoms and it has some features that distinguish it from the *c*-stacked layers. In particular the HTB arrangement of octahedra does not involve significant tilting as occurs in the *c*-stacked Ta_3Ca layers. As a result some of the HTB bridging oxygen atoms lie almost in the plane of the Ta atoms and have 3 + 1 coordination with one much longer distance, rather than tetrahedral coordination as occurs in fluorite-type phases. This in turn has an influence on the coordination of the Ca atoms in the Ca_3Ta layers on either side of the *h*- Ta_3Ca with Ca(51) having 7-coordination and others have 7 + 1 or 6 + 2 coordination as shown in Table 5.

5M $Ca_2Ta_{1.8}Nb_{0.2}O_7$ Structure

A polyhedral representation of the structure of 5M $Ca_2Ta_{1.8}Nb_{0.2}O_7$ projected along the *b* axis is shown in Fig. 5. As in the diagram of the 7M polytype, the octahedra in the *h*-stacked HTB layers are shown in dark shading. The *h*-stacked layers divide the structure into two blocks of *c*-stacked layers containing two 6 Å repeating units and three units respectively $\equiv$ 2M and 3M blocks. The metal atom

TABLE 5
Polyhedral Distances (Å) for 7M $Ca_2Ta_2O_7$

TaO_6 octahedra				CaO_n polyhedra			
Atom	⟨M–O⟩	M–O range	Layer type	Atom	Coordination	⟨M–O⟩	M–O range
Ta(1)	2.00	1.98–2.10	*cis*-Ca_3Ta	Ca(1)	8	2.59	2.45–2.74
			”	Ca(11)	8	2.57	2.29–2.84
Ta(2)	1.96	1.93–2.01	*c*-Ta_3Ca	Ca(2)	8	2.55	2.16–2.96
Ta(21)	1.96	1.94–1.99	”				
Ta(22)	1.99	1.96–2.01	”				
Ta(3)	1.98	1.96–2.02	*trans*-Ca_3Ta	Ca(3)	8	2.61	2.39–2.97
			”	Ca(31)	7 + 1	2.62	2.40–2.86 + 3.06
			”	Ca(32)	7 + 1	2.58	2.23–2.79 + 3.04
Ta(4)	1.97	1.92–1.99	*h*-Ta_3Ca	Ca(4)	8	2.54	2.21–2.85
Ta(41)	1.98	1.92–2.05	”				
Ta(42)	1.98	1.92–2.07	”				
Ta(5)	2.00	1.90–2.13	*cis*-Ca_3Ta	Ca(5)	8	2.59	2.40–2.79
			”	Ca(51)	7	2.50	2.27–2.69
			”	Ca(52)	6 + 2	2.60	2.33–2.71 + 2.97, 3.02
Ta(6)	1.97	1.92–2.02	*c*-Ta_3Ca	Ca(6)	6 + 2	2.54	2.16–2.58 + 2.83, 2.97
Ta(61)	1.98	1.95–2.00	”				
Ta(62)	1.97	1.96–1.98	”				
Ta(7)	1.99	1.90–2.14	*cis*-Ca_3Ta	Ca(7)	8	2.58	2.30–2.81
			”	Ca(71)	8	2.60	2.47–2.77
			”	Ca(72)	8	2.57	2.31–2.81
Ta(8)	1.98	1.96–2.00	*c*-Ta_3Ca	Ca(8)	8	2.54	2.17–2.89
Ta(81)	1.97	1.94–1.99	”				

layer stacking sequence is *hccchccccch* ... . The isolated octahedra in the Ca_3Ta layers in the 5M polytype all have a *cis* configuration of the pairs of nonbridging oxygen atoms.

Polyhedral bond lengths for 5M $Ca_2Ta_{1.8}Nb_{0.2}O_7$ are given in Table 6. The observed mean distances and ranges of polyhedral Ta–O and Nb–O distances are similar to those found in the 7M polytype. The largest octahedral distortion occurs for Ta(1) in the *cis*-Ca_3Ta layer in the middle of the 3M block, see Fig. 5. The distortion is associated with a large displacement of Ta towards the edge formed by the *cis*-pair of nonbridging oxygens, O(2)–O(2). As described above for the 7M polytype, the nonbridging oxygen atoms have a coordination of Ta + 3 Ca, and so the Ta displacement is to satisfy the valence requirements of O(2). The displacement results in a considerable local distortion of the close-packed metal atom array, giving chains of alternating short and long Ta(1)–Ca(11) distances, 3.44 and 3.91 Å, respectively, along [010]. This distortion of the closest packed metal atom array was also observed in the 7M polytype. We have previously reported similar distortions in other tantalate polytypes (3) and consider that they could be significant contributors to the high dielectric constants.

It is interesting to compare the structure of 5M $Ca_2Ta_{1.8}Nb_{0.2}O_7$ with that for 5M $Ca_{1.8}Ta_{1.8}Sm_{0.24}Ti_{0.17}O_7$ (3), which has the same unit cell and space group. In the Nb-doped 5M polytype both the 2M and 3M blocks have a weberite-type structure whereas in the Sm/Ti-doped 5M phase, the 2M block is of weberite-type while the 3M block is of pyrochlore-type. In the pyrochlore blocks the isolated octahedra in the Ca_3Ta layers share all 6 vertices with octahedra in the Ta_3Ca layers on either side. A comparison of the interlayer octahedral connectivity in pyrochlore-type and weberite-type blocks is illustrated in Fig. 6. The two polytypes differ only by the interchange of a single Ta/Ca pair in the metal atom framework. The relevant atoms are Ca(23) and Ta(22). As seen from Fig. 6 this has the effect of interchanging [010] rows of Ta atoms and rows of alternating Ca and Ta atoms. The change from weberite/pyrochlore to weberite/weberite results in anisotropic unit cell parameter changes, with a small (− 0.1%) decrease in *a* and larger increases in *b* (+ 0.5%) and *c* (+ 0.2%). The large increase in *b* is attributed to the [010] displacements of the Ta atoms in the *cis* Ca_3Ta layers in the 3M weberite block as discussed above.

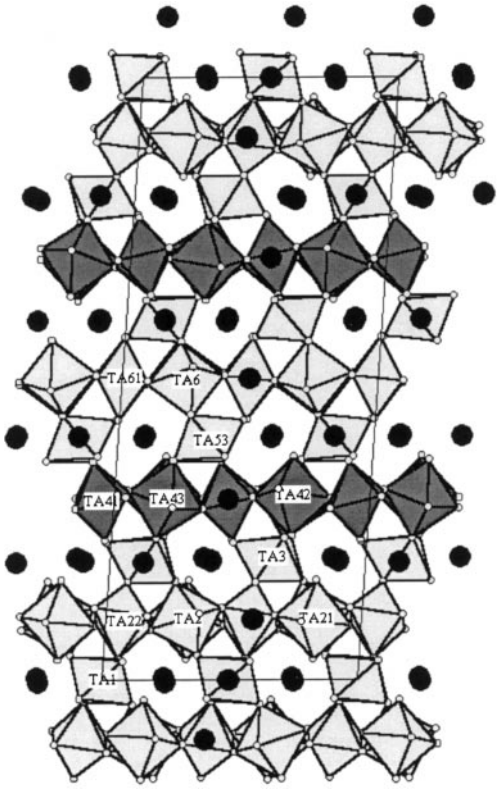

FIG. 5. [010] Projection of structure of 5M-$Ca_2Ta_{1.8}Nb_{0.2}O_7$. Dark shaded octahedra correspond to hexagonal-stacked Ta_3Ca layers. The unit cell outline is shown, c axis is vertical, Ta atoms are labelled.

Stability of 5M Polytype in the CaO–Ta_2O_5–Nb_2O_5 System

The 5M polytype of composition $Ca_2Ta_{1.8}Nb_{0.2}O_7$ was initially prepared in small batches and characterized using X-ray diffraction. We decided to prepare larger batches of the polytype for a neutron diffraction study. These were prepared in a different laboratory. Although the same preparation conditions were adhered to carefully, repeated preparations always gave the 7M polytype. However, different sources of starting materials were used and so this was investigated as a possible cause of the product variation. The different starting materials were exchanged between the two laboratories and the syntheses repeated at each laboratory. It was found that the $CaCO_3$ was responsible for the type of polytype formed. When BDH AR grade $CaCO_3$ (99.9%) was used, the 5M polytype was consistently obtained, whereas when Johnson Matthey "specpure" (99.9995%) $CaCO_3$ was used, the 7M polytype was always obtained. The two $CaCO_3$ samples were analyzed using ICP and XRF. The only significant contaminant was 0.20 wt% MgO in the BDH sample.

A test was conducted in which the equivalent of 0.2 wt% MgO was added to the specpure $CaCO_3$ in the form of a solution of $Mg(NO_3)_2$, which was then evaporated to dryness. The MgO-spiked $CaCO_3$ was used to prepare $Ca_2Ta_{1.8}Nb_{0.2}O_7$. A powder XRD pattern of the 1550°C reaction product showed single-phase 5M. The 7M polytype was formed in the absence of MgO-spiking of the specpure $CaCO_3$, thus confirming that the 5M polytype was stabilized by MgO impurity in the $CaCO_3$, When the

TABLE 6
Polyhedral Distances (Å) for 5M $Ca_2Ta_{1.8}Nb_{0.2}O_7$

TaO_6 octahedra				CaO_n polyhedra			
Atom	⟨M–O⟩	M–O range	Layer type	Atom	Coordination	⟨M–O⟩	M–O range
Ta(1)	2.03	1.98–2.15	*cis*-Ca_3Ta	Ca(11)	8	2.57	2.37–2.74
			”	Ca(12)	8	2.62	2.23–2.96
Ta(2)	1.96	1.93–2.00	*c*-Ta_3Ca	Ca(23)	7 + 1	2.50	2.10–2.96 + 2.95
Ta(21)	1.97	1.96–2.01	”				
Ta(22)	1.98	1.93–2.01	”				
Ta(3)	1.99	1.95–2.04	*cis*-Ca_3Ta	Ca(31)	7 + 1	2.61	2.23–2.86 + 3.08
			”	Ca(32)	7	2.50	2.26–2.72
			”	Ca(33)	8	2.58	2.36–2.83
Ta(41)	1.97	1.95–2.02	*h*-Ta_3Ca	Ca(4)	8	2.52	2.15–2.85
Ta(42)	1.99	1.93–2.08	”				
Ta(43)	1.99	1.95–2.04	”				
Ta(53)	2.01	1.90–2.11	*cis*-Ca_3Ta	Ca(5)	8	2.56	2.36–2.72
			”	Ca(51)	7	2.55	2.27–2.90
			”	Ca(52)	7 + 1	2.57	2.27–2.78 + 3.09
Ta(6)	1.97	1.93–2.04	*c*-Ta_3Ca	Ca(62)	8	2.50	2.14–2.88
Ta(61)	2.00	1.95–2.07	”				

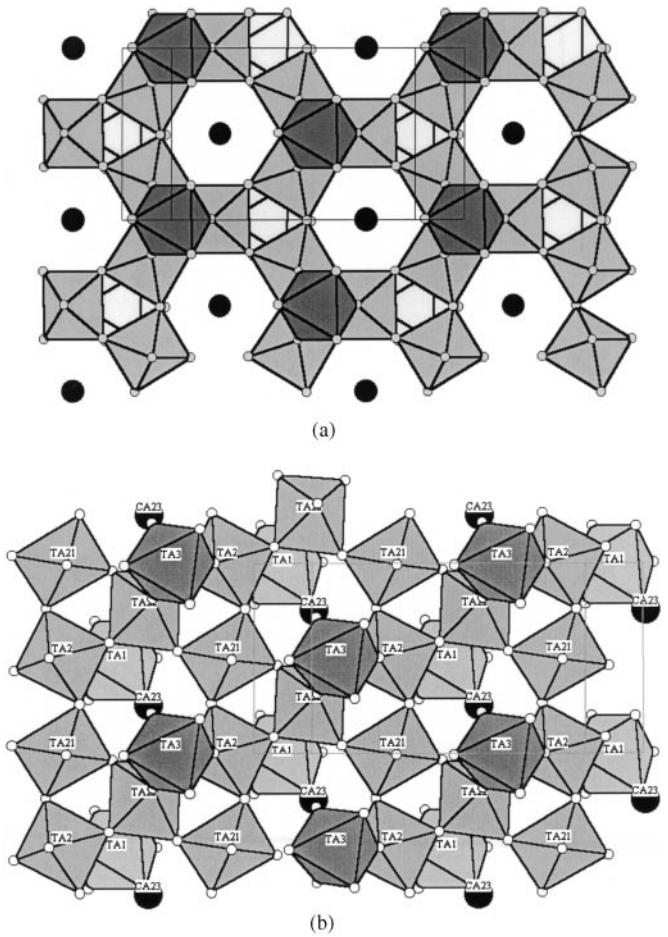

FIG. 6. (a) (001) Slice through pyrochlore block in 5M-$Ca_{1.8}Ta_{1.8}Sm_{0.24}Ti_{0.17}O_7$, showing Ta_3Ca layer with connections to octahedra above and below, (b) equivalent slice through weberite block of 5M-$Ca_2Ta_{1.8}Nb_{0.2}O_7$. Metal atoms are labelled. View is along [001], the *b* axis is vertical.

magnesia-free $CaCO_3$ was used, it was found that the 7M polytype was the stable polytype above 1400°C for all dopant levels of $Ca_2Nb_2O_7$ up to the formation of the two-phase 7M + $Ca_2Nb_2O_7$ phase region.

Dielectric Properties

Complex permittivity curves are shown in Fig. 7. Table 7 summarizes the numerical data. The general trends are as follows:

— the real part ε' is almost constant in the radio frequency (RF) range and up to a few GHz and has a mean value between 18 and 19;
— the imaginary part ε'' is not well determined but is around 0.1; the quality factor $Q = \varepsilon'/\varepsilon''$ is thus of order 200;
— above 5 GHz all samples exhibit an increase of ε' (see Fig. 8) the amplitude of which being variable and rather large for 7M $Ca_2Ta_{1.9}Nb_{0.1}O_7$ ($\Delta\varepsilon' > 10$). There is a maximum around 8 GHz and a subsequent slow decrease. Data above 12 GHz are too noisy for proper analysis.

To our knowledge, no wideband measurements of the dielectric properties of similar systems have been published

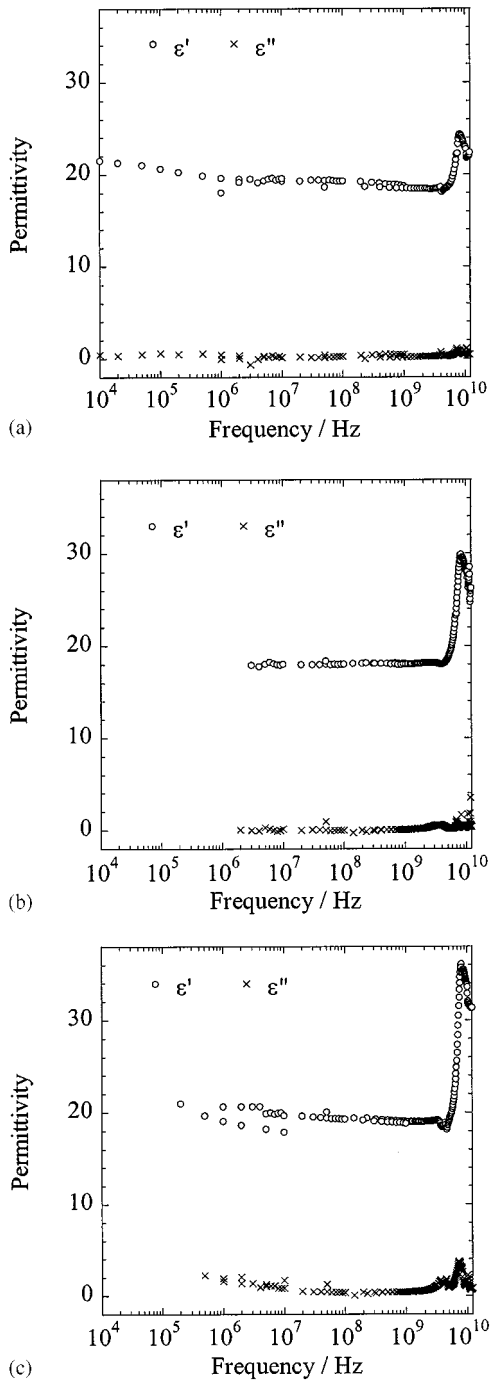

FIG. 7. Wide-band dielectric permittivity of (a) 3T Nd, Zr-doped $Ca_2Ta_2O_7$, (b) 5M $Ca_2Ta_{1.8}Nb_{0.2}O_7$, (c) 7M $Ca_2Ta_{1.9}Nb_{0.1}O_7$.

TABLE 7
Dielectric Data

	3T Nd, Zr-doped $Ca_2Ta_2O_7$	5M $Ca_2Ta_{1.8}Nb_{0.2}O_7$	7M $Ca_2Ta_{1.9}Nb_{0.1}O_7$
Thickness/mm	2.920 ± 0.01	2.220 ± 0.02	1.953 ± 0.002
ε^*(0.1–1 GHz)	18.6 + j 0.1	18.0 + j 0.05	19.0 + j 0.3
f_0/GHz	7.30 ± 0.05	7.02 ± 0.02	6.85 ± 0.03
$\varepsilon'(f_0)$	22.0 ± 0.3	24.5 ± 0.2	26.1 ± 0.3

in the literature. The RF dielectric constant of $Ca_2Ta_{2-x}Nb_xO_7$ was found (1) to be enhanced for a wide range of x values ($0.05 \leq x \leq 1.6$) as compared to pure compounds ($x = 0$ or 2): from $\varepsilon' \approx 25$ to $\varepsilon' \approx 35$. A resonant method (cavity perturbation at ca. 9.5 GHz) was used (13) to study another family of Ca ceramics with perovskite structure, $Ca(M^{3+}_{0.5}M^{5+}_{0.5})O_3$ with M^{3+} a trivalent atom and M^{5+} = Ta or Nb: ε' is in the 19.6–21 range. The correlation between ε' and the density ρ was shown to be $\Delta\varepsilon'/\varepsilon' \approx 1.5\,\Delta\rho/\rho$. It is thus difficult to ensure that the small variation between samples ($\Delta\varepsilon' \approx 0.5$) does reflect variations between their structures rather than a porosity effect.

Contributions to the dielectric permittivity are of electronic and ionic origin. The ionic polarization does change with the ion type and the packing—the more ideal the packing, the lower ε' (13, 14). Increase of ε' with frequency is found in Ba ceramics (14) above the lowest polar phonon mode damping (200 to 900 GHz) in accordance with a simple harmonic oscillator model. But no data are available between 1 MHz and 10 GHz. It is likely that Ca ceramics behave similarly, with an overall lower permittivity (13).

Due to the thickness of the samples of calcium tantalate polytypes studies here, their admittance $Y^* = G + jB$ shows at least one resonance in the microwave region.

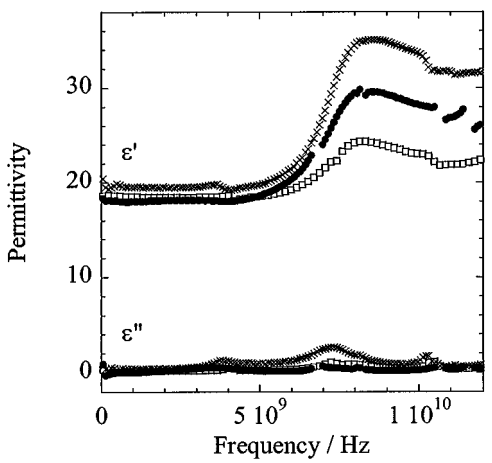

FIG. 8. Microwave permittivity of (□) 3T Nd, Zr-doped $Ca_2Ta_2O_7$, (●) 5M $Ca_2Ta_{1.8}Nb_{0.2}O_7$, (×) 7M $Ca_2Ta_{1.9}Nb_{0.1}O_7$.

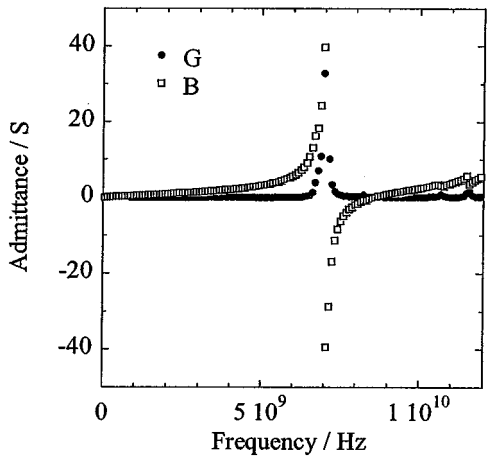

FIG. 9. Resonance of the admittance of 5M $Ca_2Ta_{1.8}Nb_{0.2}O_7$ due to its high permittivity and its thickness.

The example of 5M $Ca_2Ta_{1.8}Nb_{0.2}O_7$ is shown in Fig. 9. There is a maximum in conductance G and the sign of susceptance B changes abruptly. The resonance frequency f_0, given by $B(f_0) = 0$ is well defined and its value is given in Table 7. In the range $16 \leq \varepsilon' \leq 36$ and 1.5 mm $\leq d \leq 3$ mm, (d, ε') can be perfectly fitted to a bilinear function of $1/d$ and $1/\sqrt{\varepsilon'}$. The dependence on ε' is much stronger than that on d. Moreover, f_0 is almost insensitive to ε'' for low values, with $\Delta f_0 = 0.4\%$ if ε'' is changed from 0 and 1, the latter being higher than any experimental value. These effects allow us to determine precisely the value of ε' at frequency f_0, and these are given in Table 7.

The values of the dielectric constant at the resonant frequency are similar to those of other materials used or being considered for use in microwave communications applications. However, the low quality factors of ~ 200 mean that high dielectric losses will occur in the calcium tantalates and this will severely limit their applications.

ACKNOWLEDGMENTS

We thank Gary Fallon (Chemistry Department, University of Melbourne) for collecting the single-crystal intensity data for 7M $Ca_2Ta_2O_7$, Qing Huang (NIST, Washington) for collecting the neutron powder intensity data, and Grigor Kapoujyan (CNRS, Grenoble) for machining the pellets of the tantalate polytypes for dielectric measurements. I.E.G. acknowledges support from the Universite Joseph Fourier at Grenoble during part of this study.

REFERENCES

1. R. J. Cava, J. J. Krajewski, and R. S. Roth, *Mater. Res. Bull.* **33,** 527 (1998).
2. I. E. Grey, R. S. Roth, G. Mumme, L. A. Bendersky, and D. Minor, MRS Special Publication Volume 547, "Solid State Chemistry of Inorganic Materials II" (1999).

3. I. E. Grey and R. S. Roth, *J. Solid State Chem.* **150,** 167 (2000).
4. W. Verscharen and D. Babel, *J. Solid State Chem.* **24,** 405 (1978).
5. G. M. Sheldrick, "SHELX93, Program for the Refinement of Crystal Structures." Univ. Gottingen, 1993.
6. R. J. Hill and C. J. Howard, *J. Appl. Crystallogr.* **18,** 173 (1985).
7. D. B. Wiles and R. A. Young, *J. Appl. Crystallogr.* **14,** 149 (1981).
8. G. Cagliotti, A. Paoletti, and F. P. Ricci, *Nucl. Instrum.* **3,** 223 (1958).
9. A. L. Speck, *Acta Crystallogr. Sect. A* **46,** C-34 (1990).
10. R. A. Waldron, *in* "Theory of Guided Electromagnetic Waves," pp. 483–493. Van Nostrand Reinhold, London (1969); N. Belhadj-Tahar and A. Fourrier-Lamer, *IEEE Trans. MTT* **34,** 346 (1986).
11. K. Yagi and R. S. Roth, *Acta Crystallogr. Sect. A* **34,** 765 (1978).
12. G. Yakubovich, V. Urusov, W. Massa, G. Frenzen, and D. Babel, *Z. Anorg. Allg. Chem.* **619,** 1909 (1993).
13. M. Takata and K. Kageyama, *J. Am. Ceram. Soc.* **72,** 1955 (1989).
14. R. Zurmühlen, J. Petzelt, S. Kamba, G. Kozlov, A. Volkov, B. Gorshunov, D. Dube, A. Tagantsev, and N. Setter, *J. Appl. Phys.* **77,** 5351 (1995).